ORIGINAL RESEARCH ARTICLE

Effect of Powder Particle Size on Microstructure and Mechanical Properties of Cold-Sprayed Pure Nickel Coatings

Zhengmao Zhang[1] · Yaxin Xu[1] · Wenya Li[1] · Jingwen Yang[1] · Chunjie Huang[2]

Abstract In this study, the effect of particle size on the microstructure and mechanical properties of cold-sprayed nickel coatings was investigated using three particle size ranges of pure nickel powders. The experimental results show that the mechanical properties of the coating fabricated by the fine powder with a D_{50} of 25 μm are lower (microhardness and tensile strength of 257.5 $HV_{0.1}$ and 126 MPa, respectively) compared to those from the coarser particle sizes ($D_{50} = 45$ μm and 67 μm) because of the higher yield strength of powder, which makes it difficult to generate sufficient plastic deformation during the spraying process. The powder with the largest particle size, D_{50} of 67 μm, has a low impact velocity, which does not allow for a high-quality coating due to less plastic deformation, and the porosity is higher up to 0.7%. When the mean particle size of the powder is 45 μm, the coating shows the highest degree of densification, the porosity is 0.4%, and the mechanical properties of the coating are better with the microhardness and tensile strength of 289.2 $HV_{0.1}$ and 208 MPa, respectively.

Keywords cold spray · mechanical properties · microstructure · nickel · powder particle size

✉ Yaxin Xu
  xu.yaxin@nwpu.edu.cn

✉ Wenya Li
  liwy@nwpu.edu.cn

1 Shaanxi Key Laboratory of Friction Welding Technologies, State Key Laboratory of Solidification Processing, Northwestern Polytechnical University, Xi'an 710072, Shaanxi, China

2 Institute of Materials Technology, Helmut-Schmidt-University/University of the Federal Armed Forces Hamburg, 22043 Hamburg, Germany

Introduction

Nickel (Ni) is widely used in various corrosive industrial applications such as petrochemical, energy power and marine engineering due to its excellent corrosion resistance (Ref 1, 2). However, traditional Ni coating preparation methods such as electroplating and thermal spraying (Ref 3-5) have their limitations. Electroplating produces strongly acidic and alkaline chemical wastes that are harmful to the environment. At the same time, thermal spraying techniques (e.g., high velocity oxy-fuel spraying and plasma spraying) cause coating oxidation and grain growth due to powder melting, which seriously affects the overall performance of the coating and reduce its service life. Therefore, there is an urgent need to find an alternative process for preparing Ni coating.

Cold spray (CS) is a particle accumulation deposition process based on gas–solid two-phase hydrodynamics and high-speed impact dynamics. The principle of CS is to utilize low-temperature and high-pressure gas to accelerate the metal powder particles in a Laval nozzle, which are then caused to impact at high speeds on the substrate. As a consequence, the powder particles are deposited and a coating is formed when specific deformation conditions are reached (Ref 6-10). CS offers a viable new method for the preparation of Ni coating due to its low heat input, high deposition efficiency and ease of operation (Ref 11-17).

Particle size is a key factor influencing the acceleration and impact behavior of particles, which has a significant impact on the critical velocity required for particle deposition, and the microstructure and properties of the cold-sprayed coatings (Ref 7). Schmidt et al. (Ref 18) investigated the effect of particle size on the critical and impact velocities through the numerical simulation, and indicated that the critical velocity of particles decreases as particle
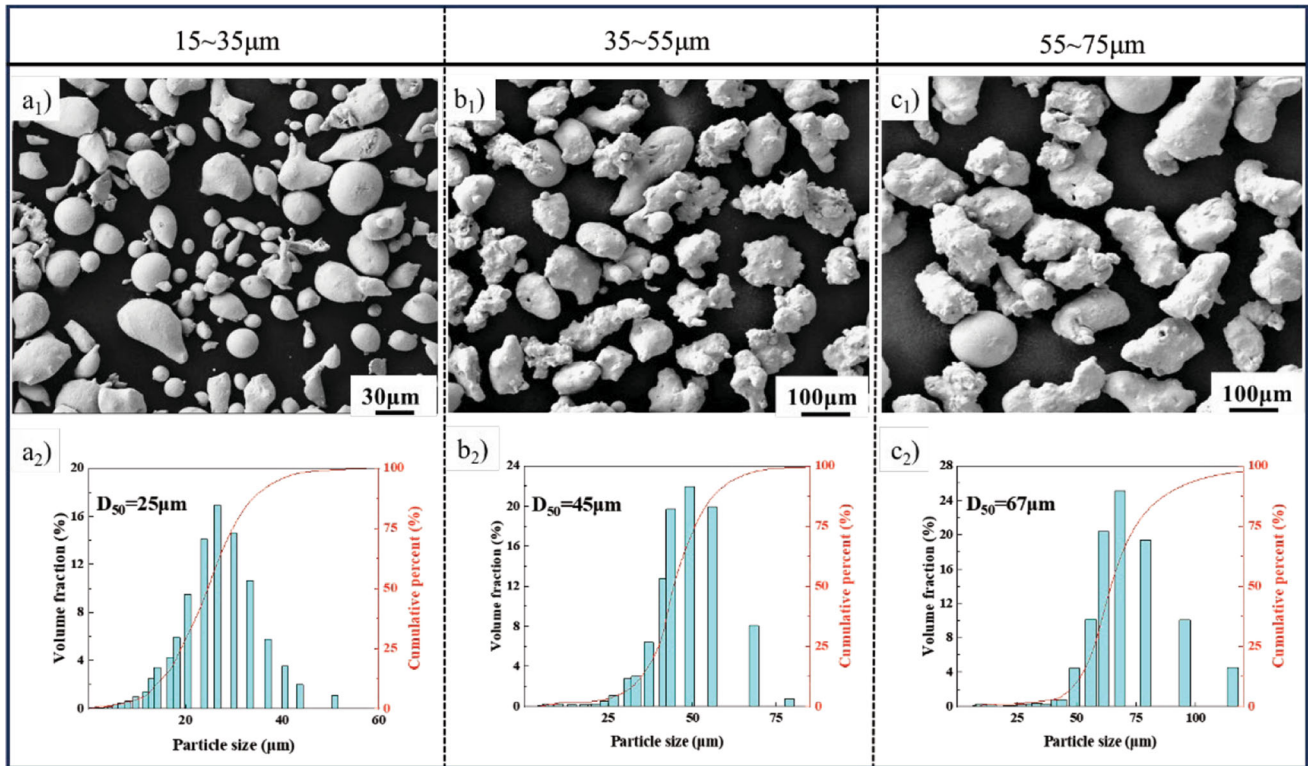
Fig. 1 Morphology and powder size distribution of three used Ni powders: (a₁, a₂) 15-35 μm, (b₁, b₂) 35-55 μm, (c₁, c₂) 55-75 μm (Color figure online)

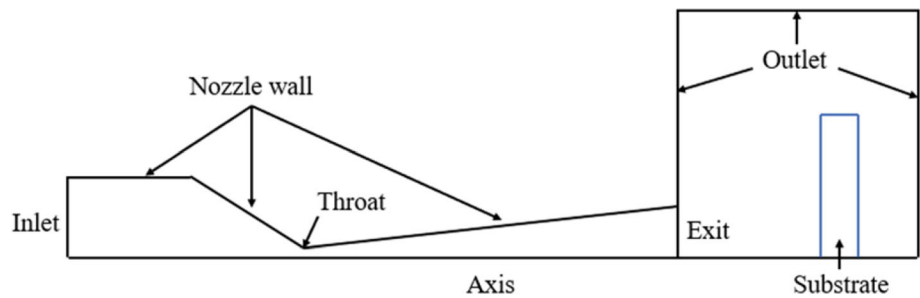**Fig. 2** Schematic diagram of nozzle calculation zone (Color figure online)

Table 1 The dimensions of the Laval nozzle

Inlet diameter, mm	Throat diameter, mm	Exit diameter, mm	Premix room length, mm	Upstream length, mm	Downstream length, mm	Expansion ratio
20	2.7	7.62	90	30	220	7.96

size increases, and the impact velocity firstly increases and then decreases. As a result, an optimal size of 10-45 μm was thus reported (Ref 18). Bae et al. (Ref 19) found that the microhardness of spherical Ni coatings decreases with increase in particle size under the same spraying conditions.

The effect of powder morphology on the deposition behavior of cold-sprayed Ni coatings has also been studied. Luo et al. (Ref 20) showed that irregularly shaped electrolytic Ni powder was easier to deposit and the resulting

coating was denser compared to spherical powder. On the contrary, Wei et al. (Ref 21) found that coating sprayed with spherical Ni powder had higher bond strength and corrosion resistance under the same spraying conditions.

However, results obtained from different researchers have varied, indicating that the performance of cold-sprayed coatings is not only affected by powder parameter, such as powder strength, powder size and oxide film on the surface of the particles (Ref 22), but also depends on various factors, such as the spraying gas parameters (Ref 23),

Fig. 3 The sampling position and size of tensile specimen: (a) the sampling position, (b) the size of tensile specimen (Color figure online)
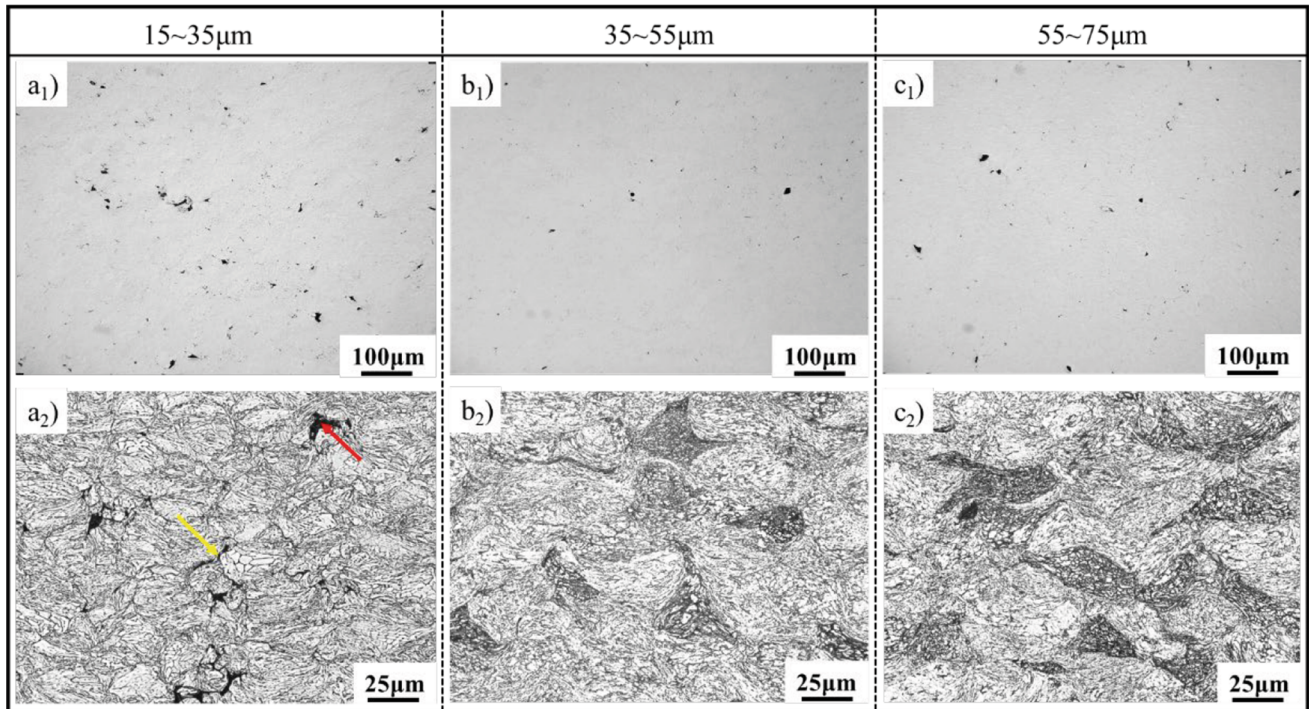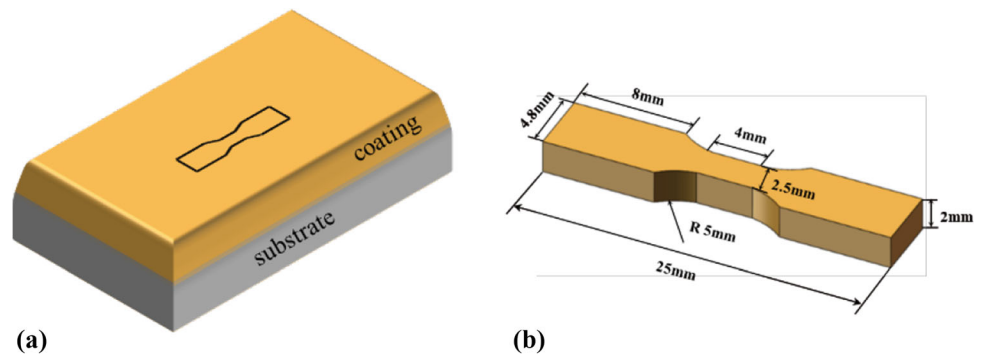

Fig. 4 Cross-sectional microstructures of Ni coatings deposited with different particle sizes: (a₁, a₂) 15-35 μm, (b₁, b₂) 35-55 μm, (c₁, c₂) 55-75 μm; (a₁-c₁) cold sprayed, (a₂-c₂) etched (Color figure online)

and the nozzle specifications (Ref 24). Zhang et al. (Ref 25) found that an increase in working gas temperature significantly improved the coating densification and thus the coating bonding strength. In order to promote the wide application of cold-sprayed Ni coatings, this study further focuses on the effect of irregular Ni powder particle size on the coating quality.

Experimental Procedures

The used powder feedstock in this study was irregular Ni powder with purity ≥ 99.5%. The morphology of the three powders is shown in Fig. 1(a₁-c₁), as observed by scanning electron microscopy (SEM, TESCAN VEGA 3 LMU, Czech). The average particle sizes (D₅₀) of the used Powder 1 (15-35 μm), Powder 2 (35-55 μm) and Powder 3 (55-75 μm) were 24, 45 and 67 μm, respectively, as shown in Fig. 1(a₂-c₂). The substrate material was pure Ni plate, which was sandblasted prior to spraying. The cold spray experiments were carried out by using a homemade CS system (NPU, Xi'an, China). The working gas pressure and temperature were 3.8 MPa and 600 °C, respectively. The spraying distance was 30 mm, and the nozzle transverse speed was 20 mm/s.

The computational fluid dynamics (CFD) software ANSYS/Fluent was used to predict the impact velocity of Ni particles at different particle sizes. A two-dimensional axisymmetric model was used in this study as shown in Fig. 2. The model consists of symmetry axis, nozzle inlet, nozzle outlet, nozzle wall, substrate surface and outlet. The specific dimensions of the Laval nozzle are shown in
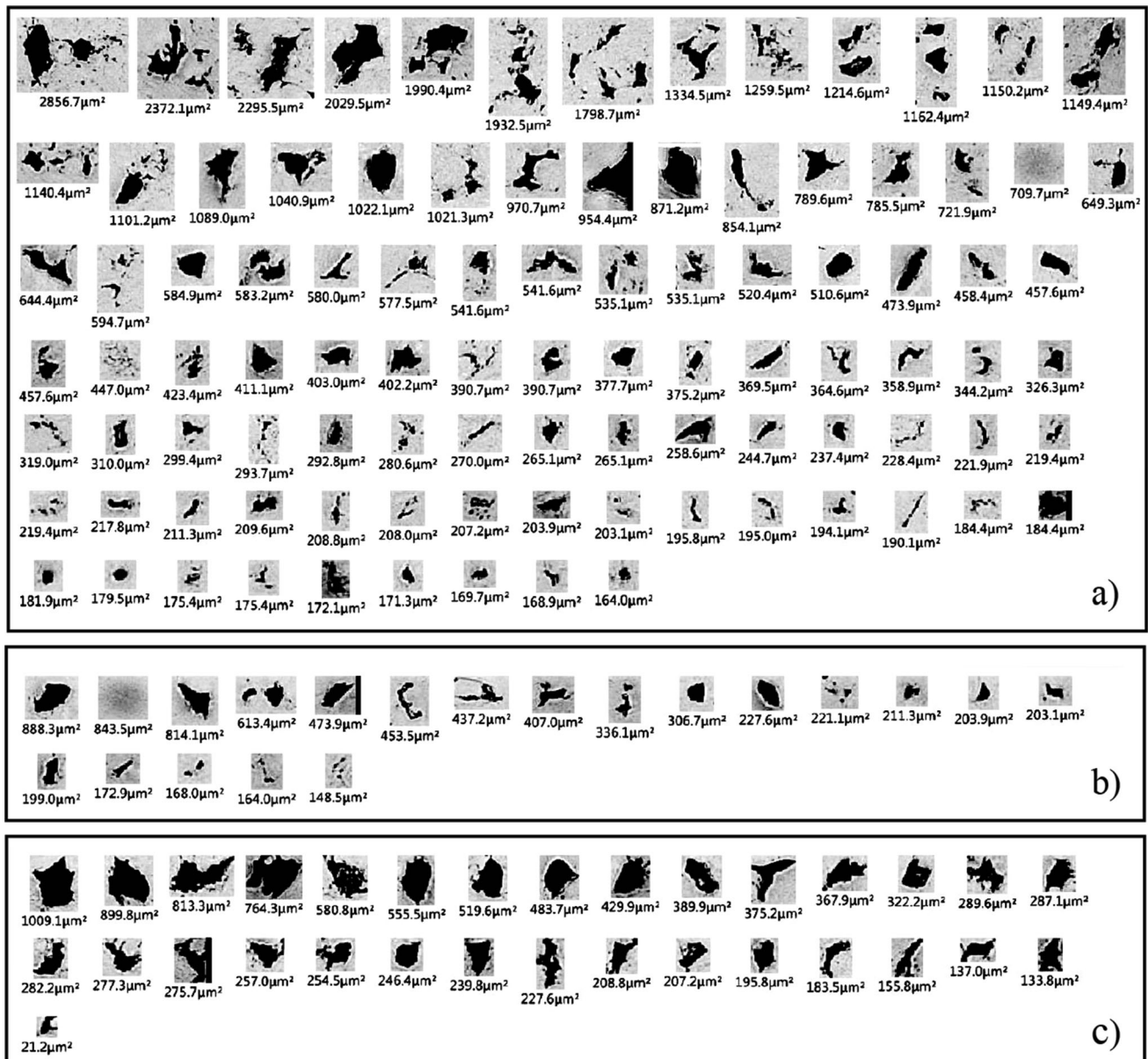
Fig. 5 Defect distribution of Ni coatings deposited with different particle sizes: (a) 15-35 μm, (b) 35-55 μm, (c) 55-75 μm

Table 1. The working gas used in the calculation is the same as the parameters of CS experiments in this study. The temperature and pressure of the working gas are 600 °C and 3.8 MPa, respectively. The spraying distance is 30 mm. The particle sizes correspond to the average particle sizes of Powder 1, Powder 2 and Powder 3 used in the spraying process, which are 24, 45 and 67 μm, respectively.

The cross section of the obtained Ni coating was analyzed using an optical microscope (OM, KEYENCE VHX-5000, Japan) and the porosity was measured using the Image Pro Plus software (V6.0, America). The etching agent for revealing the coating microstructure was prepared by mixing 40 %HNO$_3$ and 60 % CH$_3$COOH. The

microstructural details were analyzed by electron backscatter diffraction (EBSD, ZEISS Gemini 300, Germany). The EBSD data was assessed at 15 kV with a step size of 0.2 μm and processed into image quality (IQ), grain boundaries (GBs), inverse pole figure (IPF) and kernel average misorientation (KAM) maps. The microhardness of coatings was tested by LECO electronic microhardness tester (AMT-43, America) with a load of 100 g and a holding time of 15 s. The tensile test was carried out by an INSTRON electronic universal mechanical testing machine ((3382, America) with a tensile speed of 0.12 mm/s. The dimensions of the tensile samples are shown in Fig. 3, and the extensometer is not used in the tensile test.

Results and Discussion

Coating Defect Characteristics and Porosity

Figure 4 depicts the OM cross-sectional microstructures of Ni coatings deposited with different particle sizes. As shown in Fig. 4(a_1), the Ni coating under Powder 1 condition exhibits obvious internal defects with a porosity of about 2.3%. In contrast, the microstructure of the Ni coating under Powder 2 condition (Fig. 4b_1) is the densest with a porosity of about 0.4%. Figure 4(c_1) shows the microstructure of the Ni coating deposited with Powder 3, which is significantly better than that of Powder 1, although the compactness of the coating is lower than that of Powder 2, with a porosity of about 0.7%. From the etched morphologies of the Ni coatings shown in Fig. 4(a_2-c_2), it can be seen that the defects in the cold-sprayed coatings are mainly divided into two categories: large pores (see red arrow in Fig. 4a_2) and small non-bonded interfaces between particles (see yellow arrow in Fig. 4a_2).

The defect characteristics, including defect size, content and distribution, are crucial factors that influence the quality of coatings. Quantifying the number and size of defects in Ni coatings can facilitate further investigation of the influence of defect characteristics on the mechanical properties of Ni coatings. Figure 5 shows the defect feature maps extracted by OM from the coating cross sections, corresponding to Fig. 4(a_1-c_1). The defect areas of Ni coatings deposited with different powder sizes account for 2.7%, 0.5% and 0.9% of the total coating area, respectively, which is consistent with the porosity of Ni coatings obtained by digital image processing (Fig. 6).

The results of particle compression test indicate that the strength of metal powder increases with decrease in particle sizes (Ref 26, 27). Specifically, Powder 1, which has the smallest particle size range, has the highest yield strength due to its significant internal strain strengthening effect that enhances the ability of the particles to resist plastic deformation upon impact the substrate. On the other hand, the critical velocity of the particles decreases with increase in particle size (Ref 18), which also leads to the fact that the fine powder is more difficult to deposit than larger ones. Therefore, under the same spray conditions, it is difficult for Powder 1 to undergo large plastic deformation, and a good interfacial bonding cannot be formed between the particles, thus resulting in the highest number of defects in the deposited coating. On the contrary, when the particle size range of the Ni powder is increased from 15-35 μm to 35-55 μm, the deformation resistance of the powder was reduced, which leads to server plastic deformation and thus denser coatings. A study by Ajdelsztajn et al. (Ref 28) showed that the impact velocity of the
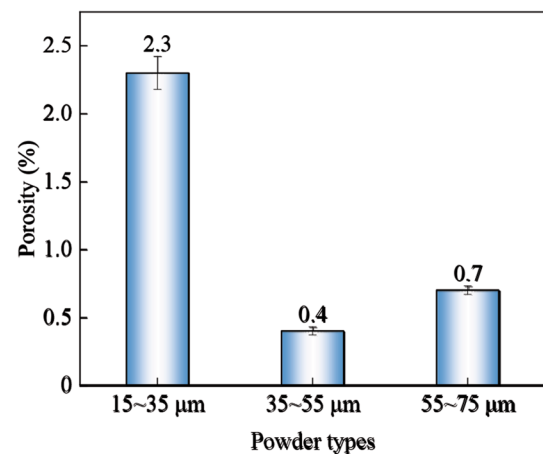

Fig. 6 Porosity of Ni coatings deposited with different particle sizes (Color figure online)
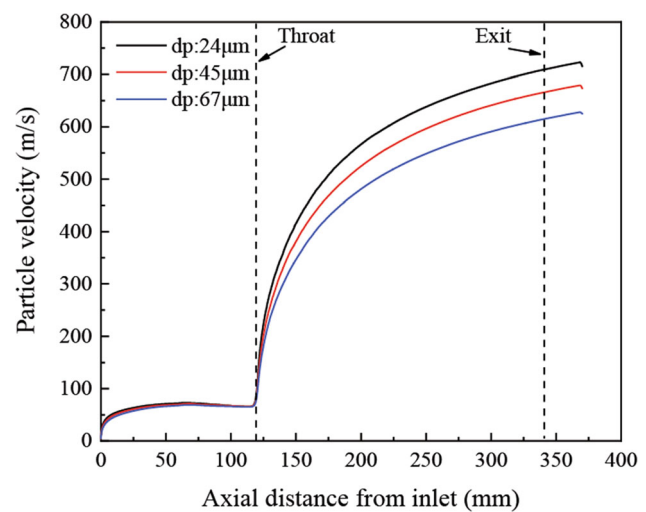

Fig. 7 Effect of particle diameter on particle acceleration behavior for the irregular Ni powders (Color figure online)

particles decreased significantly with the increase in particle size when the particle size of the powder was increased to a certain range. Figure 7 shows the acceleration behavior of irregular Ni particles with different particle sizes under the same airflow condition. As can be seen that after the particles reach the substrate, the impact velocities of Ni particles with particle diameters of 24 μm, 45 μm and 67 μm are 639 m/s, 595 m/s and 542 m/s, respectively. For Powder 3, the impact velocities are significantly lower than that of powder 2 as the particle size increases further, resulting in a higher defect distribution in the coating than that of the powder 2 condition.

Coating Microstructure

To further reveal the influence of particle size on the coating microstructures, detailed investigations of the cold-

sprayed Ni particles are needed. Figure 8 presents the EBSD data of the regions at the cross-sectional from Ni coatings with different particle sizes. From the IPF maps (Fig. 8a_1-a_3), it investigates that the Ni particles of different sizes undergo significant plastic deformation after high-speed impact with the substrate. The dynamic recrystallization-induced grain refinement results in a large number of small-sized grains at the particle bonding interface, while the internal deformation of the particles is mainly due to grain refinement caused by dislocation movement, with grain sizes significantly larger than those at the particle boundaries, and the overall crystal orientation of the coatings shows a random distribution. As shown in the grain boundary maps of Ni coatings in Fig. 8(b_1-b_3), a large number of atomic dislocations exist inside the grains at the deformation particle boundaries due to work hardening, resulting in the formation of high-angle grain boundaries and sub-grain boundaries with high grain boundary energy. Figure 8(c_1-c_3) shows the kernel average misorientation (KAM) of the Ni coatings deposited with different particle sizes. The green and red represent the regions with large strain and high dislocation density, while the blue is the region with relatively small strain rate and dislocation density. It investigates that the dislocation density at the particle boundaries is lower than that inside the particles due to the sub-grain boundaries and high-angle grain
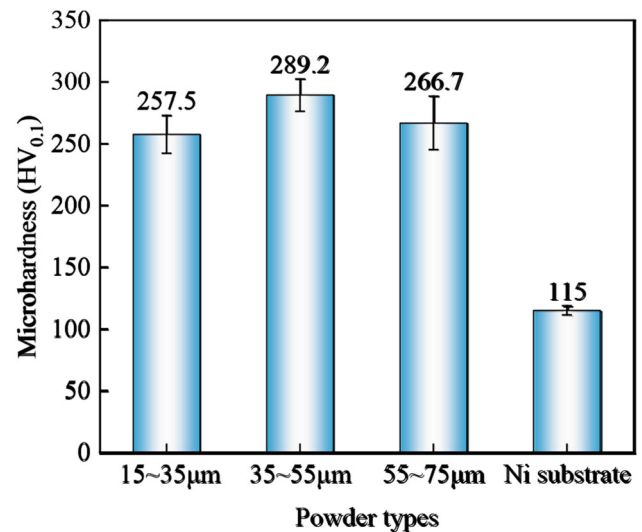
Fig. 9 Microhardness of Ni coatings deposited with different particle sizes (Color figure online)
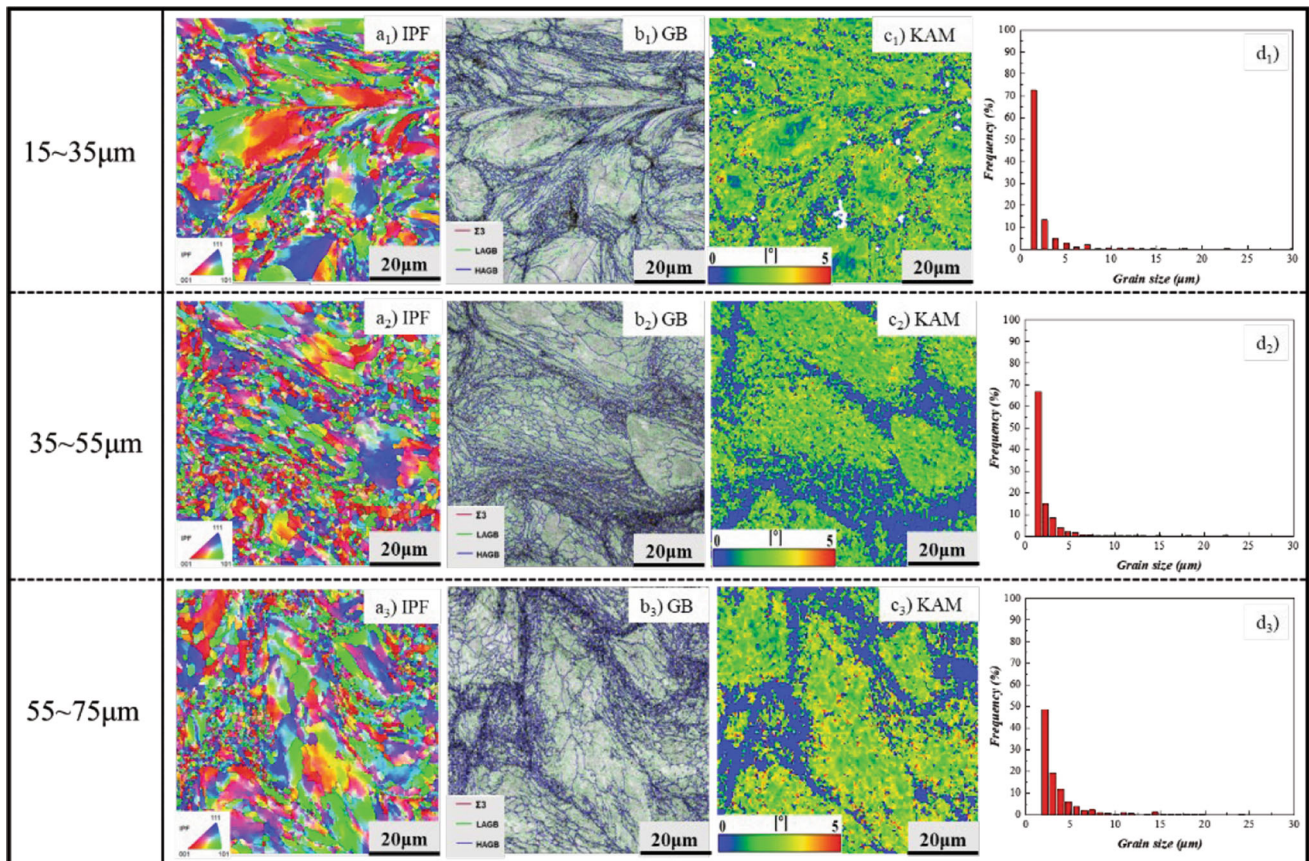
Fig. 8 EBSD data of Ni coatings deposited with different particle sizes: (a_1-a_3) IPF maps; (b_1-b_3) GB maps; (c_1-c_3) KAM maps; (d_1-d_3) grain size distribution maps; (a_1-d_1) 15-35 μm; (a_2-d_2) 35-55 μm; (a_3-d_3) 55-75 μm (Color figure online)

boundaries have a strong absorption capacity for dislocations. For the Ni coating deposited with Powder 2, the grain refinement effect of the coating is most significant, which investigates that as the particle size of Ni powder increases from 15-35 μm to 35-55 μm, the resistance to powder deformation decreases, allowing for greater plastic deformation of Ni particles, the particle boundaries show the lowest dislocation density, as shown in Fig. 8(c_2). Consequently, the overall dislocation density inside the coating decreases. However, when the particle size range further increases to 55-75 μm, the particle impact velocity significantly decreases, making it difficult for the powder to undergo sufficient plastic deformation, and the grain refinement effect of the coating after deposition weakens.

Figure 8(d_1-d_3) shows the grain size distribution of Ni coatings deposited with different powder size. It investigates that the average grain sizes of Ni coatings deposited with Powder 1, Powder 2 and Powder 3 are 1.23 μm, 1.54 μm and 2.31 μm, respectively, increasing with the powder particle size ranges increases. It is believed that the powder with a small particle size will form ultrafine grains inside the particles during the rapid cooling stage in the powder preparation process (Ref 29), resulting in significantly smaller overall grain sizes of these powder than that of the powder with a larger particle size. During cold spray process, the grain size inside the coating is further refined, so the average grain size increases with the increase in powder size.

Coatings Mechanical Properties

Microhardness

Figure 9 presents the average microhardness of Ni coatings deposited with different particle sizes. It shows that the microhardness of the Ni substrate is only 115 $HV_{0.1}$, but the Ni coatings deposited by cold spray process using Powder 1 to Powder 3 have microhardness values of 257.5 $HV_{0.1}$, 289.2 $HV_{0.1}$ and 266.7 $HV_{0.1}$, respectively, indicating a significant increase in microhardness. During cold spray, high-speed Ni powder particles impact on the substrate, causing deformation and depositing on it. The deposited particles then undergo further deformation due to the impact of subsequent particles, resulting in work hardening and higher microhardness of the Ni coating compared to the substrate. In contrast to the results reported by Bae et al. (Ref 19), the microhardness of the Ni coating obtained in this study is highest when using Powder 2 (the medium particle size range, 35-55 μm). The possible reason for this difference is the effect of powder morphologies on the number of internal defects in the obtained Ni coatings. Comparing to the coating deposited
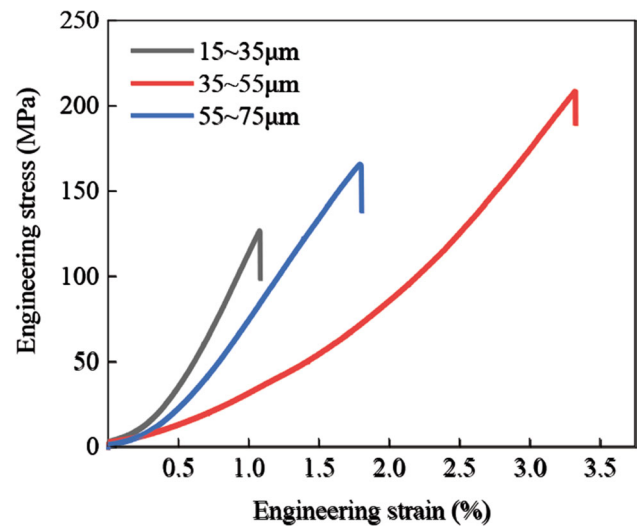

Fig. 11 Tensile stress–strain curves of Ni coatings deposited with different particle sizes (Color figure online)
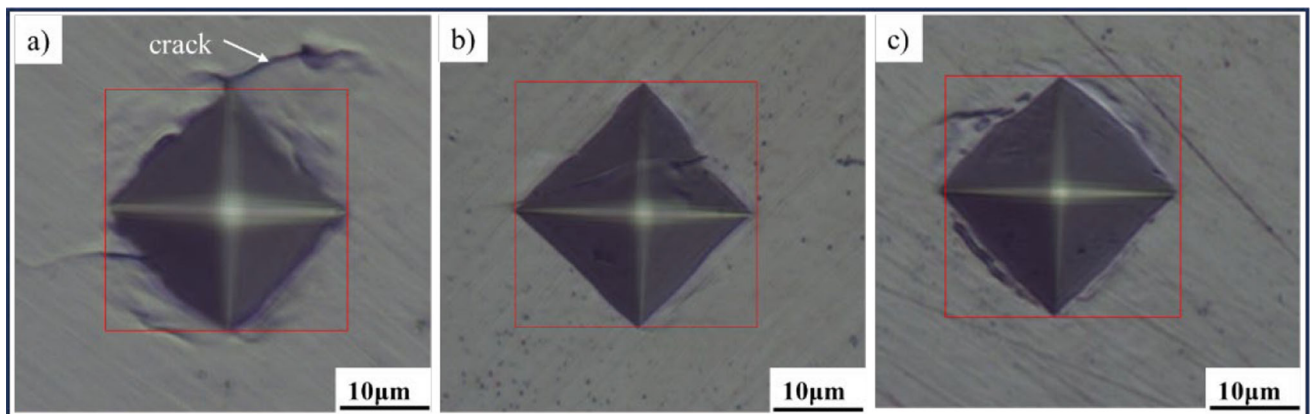

Fig. 10 The typical hardness indentation morphology of Ni coatings deposited with different particle sizes: (a) 15-35 μm; (b) 35-55 μm; (c) 55-75 μm (Color figure online)

with Powder 2, the coating deposited with Powder 1 has more internal defects with large sizes. During microhardness testing, the high compressive stress caused by the indentation locating near internal defects in the coating can cause the coating to fracture, resulting in decreased overall microhardness, as shown in Fig. 10.

Tensile test

Figure 11 illustrates the stress–strain curves of Ni coatings under different particle size conditions. It shows that the Ni coating fabricated with Powder 2 powder exhibits the highest tensile strength of 208 MPa, whereas the Ni coatings under Powder 1 and Powder 3 conditions demonstrate tensile strengths of 126 MPa and 166 MPa, respectively. To elucidate the differences in tensile test of Ni coatings with different particle size, the surface microstructures of the fractured samples are analyzed by SEM in top views, as displayed in Fig. 12. It can be seen that all coatings exhibit brittle fracture characteristics. River-like patterns are observable on the fracture surfaces, indicating that the fracture mode is brittle cleavage fracture.

For the Ni coating under Powder 1 condition, it is found that there are obvious large pore defects at the fracture surface, as shown in Fig. 12a$_2$. This indicates that the strength of the coating is closely related to the distribution of internal defects. During the tensile process, there are apparent stress concentration phenomena at the defect sites. The higher stress makes the defect sites more susceptible to become crack sources and initiate cracking. Since the Ni coating prepared with Powder 1 has the most internal defects, the coating exhibits a higher stress concentration phenomenon during the tensile process, resulting in the lowest tensile strength of the coating. For the Ni coating under Powder 2 condition, it can be observed that there are some tear lines that appear inside the particles from Fig. 12b$_2$, which is the enlarged diagram of the red box area in Fig. 12b$_1$, indicating that good metallurgical bonding is formed between most of the particles, but the whole coating still shows the characteristics of brittle fracture. From the enlarged area of the fracture under Powder 3 powder conditions shown in Fig. 12c$_2$, it can be found that there is a smooth bonding interface between some particles, indicating that the bonding between particles is also mainly mechanical bonding.

Conclusions

For the cold spraying of Ni, this study investigated the correlation between particle size and the properties of Ni coatings, and the following conclusions were drawn:

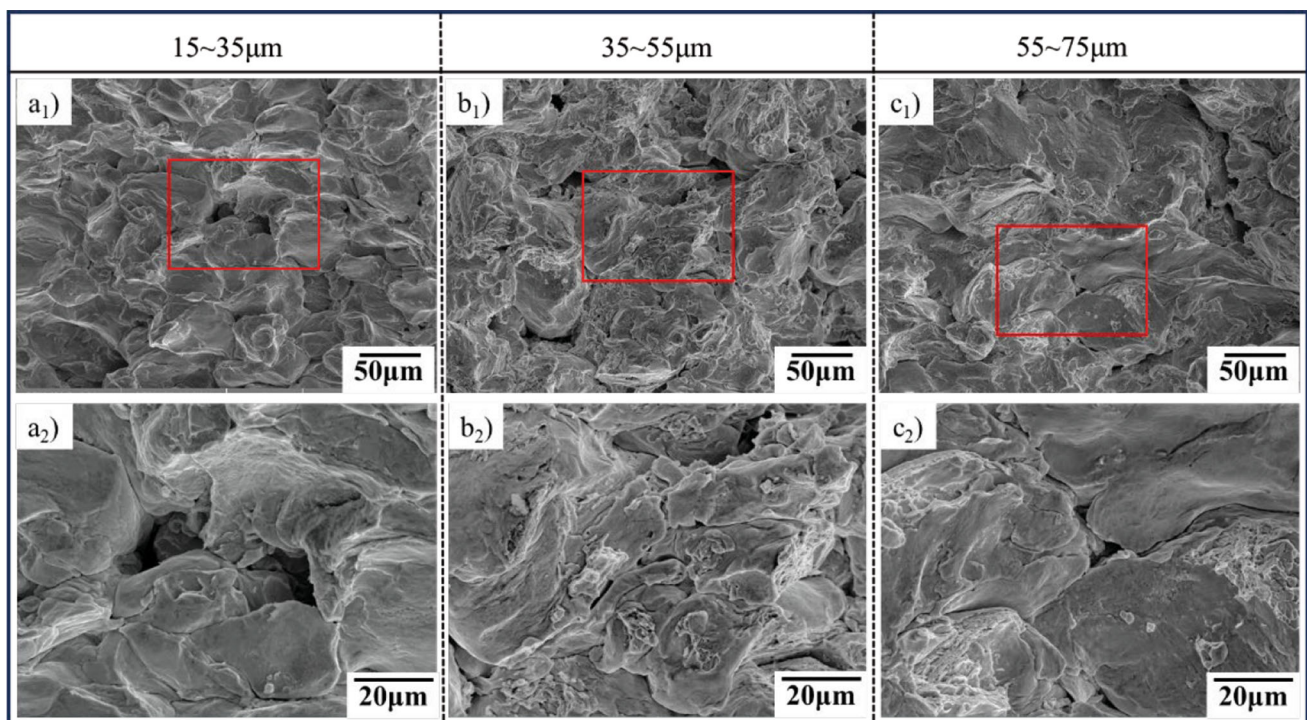(1)   Comparing the properties of Ni coatings with different powder particle sizes, the porosity of Ni

Fig. 12 Fracture surfaces of Ni coatings deposited with different particle sizes: (a$_1$, a$_2$) 15-35 μm, (b$_1$, b$_2$) 35-55 μm, (c$_1$, c$_2$) 55-75 μm; (a$_2$-c$_2$) Enlarged view of the red box in (a$_1$-c$_1$) respectively (Color figure online)

coatings deposited by Powder 1, Powder 2 and Powder 3 was 2.3%, 0.4% and 0.7% in terms of OM, respectively

(2) The 15-35 μm powder has high yield strength and plastic deformation resistance, which results in a large number of defects and non-bonded interfaces within the coating, which exhibits the worst mechanical properties, with a microhardness of 257.5 $HV_{0.1}$ and a tensile strength of 126 MPa.

(3) The Ni coating produced with the powder of 35-55 μm demonstrates the highest microhardness of 289.2 $HV_{0.1}$ and the highest tensile strength of 208 MPa.

(4) As the powder particle size increases further to 55-75 μm, the decrease in particle impact velocity leads to a decrease in the microhardness and tensile strength of the Ni coating, which are 266.7 $HV_{0.1}$ and 166 MPa, respectively.

References

1. E.S.M. Sherif, A.A. Almajid, A.K. Bairamov, and E. Al-Zahrani, Corrosion of Monel-400 in Aerated Stagnant Arabian Gulf Seawater after Different Exposure Intervals, *Int. J. Electrochem. Sci.*, 2011, **6**, p 5430-5444.

2. M.R. Zamanzad-Ghavidel, K. Raeissi, and A. Saatchi, The effect of Surface Morphology on Pitting Corrosion Resistance of Ni Nanocrystalline Coatings, *Mater. Lett.*, 2009, **63**, p 1807-1809.

3. J. Andreska, C. Maurer, J. Bohnet, and U. Schulz, Erosion Resistance of Electroplated Nickel Coatings on Carbon-fibre Reinforced Plastics, *Wear*, 2014, **319**, p 138-144.

4. J. Sudagar, J.S. Lian, and W. Sha, Electroless Nickel, Alloy, Composite and Nano Coatings—A Critical Review, *J. Alloys Compd.*, 2013, **571**, p 183-204.

5. A. Laik, D.P. Chakravarthy, and G.B. Kale, On Characterisation of Wire-Arc-Plasma-Sprayed Ni on Alumina Substrate, *Mater Charact*, 2005, **55**, p 118-126.

6. W.Y. Li, K. Yang, S. Yin, X.W. Yang, Y.X. Xu, and R. Lupoi, Solid-State Additive Manufacturing and Repairing by Cold Spraying: A Review, *J. Mater. Sci. Technol.*, 2018, **34**, p 440-457.

7. W.Y. Li, C.C. Cao, and S. Yin, Solid-State Cold Spraying of Ti and its Alloys: A Literature Review, *Prog. Mater. Sci.*, 2020, **110**, 100633.

8. C.Y. Chen, Y.C. Xie, S. Yin, W.Y. Li, X.T. Luo, X.L. Xie, R.X. Zhao, C.M. Deng, J. Wang, H.L. Liao, M. Liu, and Z.M. Ren, Ductile and High Strength Cu Fabricated by Solid-State Cold Spray Additive Manufacturing, *J. Mater. Sci. Technol.*, 2023, **134**, p 234-243.

9. C.J. Huang, W.Y. Li, Y.C. Xie, M.P. Planche, H.L. Liao, and G. Montavon, Effect of Substrate Type on Deposition Behavior and Wear Performance of Ni-Coated Graphite/Al Composite Coatings Deposited by Cold Spraying, *J. Mater. Sci. Technol.*, 2017, **33**, p 338-346.

10. C.J. Huang, M. Arseenko, L. Zhao, Y.C. Xie, A. Elsenberg, W.Y. Li, F. Gartner, A. Simar, and T. Klassen, Property Prediction and Crack Growth Behavior in Cold Sprayed Cu Deposits[J], *Mater. Des.*, 2021, **206**, 109826.

11. W.Y. Li, C. Zhang, X. Guo, C.J. Li, H. Liao, and C. Coddet, Study on Impact Fusion at Particle Interfaces and its Effect on Coating Microstructure in Cold Spraying, *Appl. Surf. Sci.*, 2007, **254**, p 517-526.

12. L. Ajdelsztajn, B. Jodoin, and J.M. Schoenung, Synthesis and Mechanical Properties of Nanocrystalline Ni Coatings Produced by Cold Gas Dynamic Spraying, *Surf. Coat. Technol.*, 2006, **201**, p 1166-1172.

13. C.J. Huang, A. List, J.J. Shen, B.L. Fu, S. Yin, T. Chen, B. Klusemann, F. Gartner, and T. Klassen, Tailoring Powder Strengths for Enhanced Quality of Cold Sprayed Al6061 Deposits[J], *Mater. Des.*, 2022, **215**, 110494.

14. Y. Zou, W. Qin, E. Irissou, J.G. Legoux, S. Yue, and J.A. Szpunar, Dynamic Recrystallization in the Particle/Particle Interfacial Region of Cold-Sprayed Nickel Coating: Electron Backscatter Diffraction Characterization, *Scr. Mater.*, 2009, **61**, p 899-902.

15. W.Y. Li, Z.M. Zhang, Y.X. Xu, Z.G. Song, and S. Yin, Research Progress of Cold Sprayed Ni and Ni-Based Composite Coatings: A Review, *Acta Metall. Sin.*, 2022, **58**, p 1-16. (in china)

16. C.J. Huang, W.Y. Li, Z.H. Zhang, M.P. Planche, H.L. Liao, and G. Montavon, Effect of Tool Rotation Speed on Microstructure and Microhardness of Friction-Stir-Processed Cold-Sprayed SiCp/Al5056 Composite Coating, *J. Therm. Spray Technol.*, 2016, **25**, p 1357-1364.

17. Y.X. Xu, J.J. Ge, B.J. Ji, and W.Y. Li, Mechanical Alloying of Cold-Sprayed Ni-Nb-Si Composite Coating by Friction Stir Processing: Improvement in Microstructure and Resistance Against Molten Silicates Corrosion, *Surf. Coat. Technol.*, 2022, **451**, 129051.

18. T. Schmidt, F. Gartner, H. Assadi, and H. Kreye, Development of a Generalized Parameter Window for Cold Spray Deposition, *Acta Mater.*, 2006, **54**, p 729-742.

19. G. Bae, K. Kang, H. Na, J.J. Kim, and C. Lee, Effect of Particle Size on the Microstructure and Properties of Kinetic Sprayed Nickel Coatings, *Surf. Coat. Technol.*, 2010, **204**, p 3326-3335.

20. X.T. Luo, Y.J. Li and, C.J. Li, A Comparison of Cold Spray Deposition Behavior Between Gas Atomized and Dendritic Porous Electrolytic Ni Powders Under the Same Spray Conditions, *Mater. Lett.*, 2016, **163**, p 58-60.

21. Y.K. Wei, X.T. Luo, X. Chu, Y. Ge, G.S. Huang, Y.C. Xie, R.Z. Huang, and C.J. Li, Ni Coatings for Corrosion Protection of Mg Alloys Prepared by an In-Situ Micro-Forging Assisted Cold Spray: Effect of Powder Feedstock Characteristics, *Corros. Sci.*, 2021, **184**, 109397.

22. W.Y. Li, C.J. Li, Y.Y. Wang, and G.J. Yang, Effect of Parameters of Cold Sprayed Cu Particles on its Impacting Behavior, *Acta Metall. Sin.*, 2005, **41**, p 282-286.

23. Y.M. Xiong, G. Bae, X. Xiong, and C. Lee, The Effects of Successive Impacts and Cold Welds on the Deposition Onset of Cold Spray Coatings, *J. Therm. Spray Technol.*, 2010, **19**, p 575-585.

24. W.P. Wan, W.Y. Li, D. Wu, Z.W. Qi, and Z.M. Zhang, New Insights into the Effects of Powder Injector Inner Diameter and Overhang Length on Particle Accelerating Behavior in Cold Spray Additive Manufacturing by Numerical Simulation, *Surf. Coat. Technol.*, 2022, **444**, 128670.

25. H.B. Zhang, J.B. Zhang, A.D. San, J.S. Wu, and H.W. Hong, Effects of Gas Temperature on Bonding and Deformation

Behavior of Cold-Sprayed Ni Particles, *Acta Metall. Sin.*, 2007, **43**, p 823-828.

26. H. Assadi, I. Irkhin, H. Gutzmann, F. Gartner, M. Schulze, M.V. Vidaller, and T. Klassen, Determination of Plastic Constitutive Properties of Microparticles Through Single Particle Compression, *Adv. Powder Technol.*, 2015, **26**, p 1544-1554.

27. H. Assadi and F. Gartner, Particle Compression Test: A Key Step towards Tailoring of Feedstock Powder for Cold Spraying, *Coatings*, 2020, **10**, p 458.

28. L. Ajdelsztajn, B. Jodoin, G.E. Kim, and J.M. Schoenung, Cold Spray Deposition of Nanocrystalline Aluminum Alloys, Metallurgical and Materials Transactions A-Physical Metallurgy and Materials, *Science*, 2005, **36A**, p 657-666.

29. T. Stoltenhoff, H. Kreye, and H.J. Richter, An Analysis of the Cold Spray Process and its Coatings, *J. Therm. Spray Technol.*, 2002, **11**, p 542-550.